arXiv:1403.2262v1 [cond-mat.supr-con] 10 Mar 2014

# The chemical physics of unconventional superconductivity

Sumit Mazumdar*, R. Torsten Clay†

March 11, 2014

**Abstract**

Attempts to explain correlated-electron superconductivity have largely focused on the proximity of the superconducting state to antiferromagnetism. Yet, there exist many correlated-electron systems that exhibit insulator-superconducting transitions where the insulating state exhibits spatial broken symmetry different from antiferromagnetism. Here we focus on a subset of such compounds which are seemingly very different in which specific chemical stoichiometries play a distinct role, and small deviations from stoichiometry can destroy superconductivity. These superconducting materials share a unique carrier concentration, at which we show there is a stronger than usual tendency to form local spin-singlets. We posit that superconductivity is a consequence of these pseudomolecules becoming mobile as was suggested by Schafroth a few years prior to the advent of the BCS theory.

*Department of Physics, University of Arizona, Tucson, AZ 85721

†Department of Physics & Astronomy and HPC$^2$ Center for Computational Science, Mississippi State University, Mississippi State, MS 39762

# INTRODUCTION

Theoretical condensed matter physicists have been searching for a theory of correlated-electron superconductivity (SC) for more than 25 years, since the discovery[1] of SC in $La_{2-x}Sr_xCuO_4$. Consensus is slowly emerging that the problem demands a conceptually new approach altogether. It is also accepted by many scientists by now that copper oxides are but only one out of many families or classes of materials in which SC is unconventional, in the sense that the SC cannot be explained within the standard BCS approach. Materials in which SC is thought to be unconventional include besides the cuprates the new Fe compounds[2], various ternary and quaternary transition metal compounds[3,4], organic charge-transfer solids[5], and perhaps also the fullerides[6] and the recently discovered metal-intercalated polycyclic aromatic hydrocarbons[7] such as phenanthrene, picene, etc. In all these cases electron-electron (e-e) interactions are believed to be strong. As shown by Uemura et al. two decades back[8], unconventional superconductors can be be identified by their large $T_c/T_F$ (here $T_F$ is the Fermi temperature). Thus while $T_c/T_F \sim 10^{-5}$ for elemental Al and Zn, and $\sim 10^{-3}$ for Nb with the highest $T_c$ among elements, the unconventional superconductors all lie within a band with $10^{-2} < T_c/T_F < 10^{-1}$ (see Fig. 3 in reference 8).

While the bulk of the theoretical effort has gone into attempts to understand the detailed behavior of individual families of materials (such as the origin of the pseudogap in the cuprates), an alternate approach involves determining *what* precisely is common between these materials *besides* strong e-e interactions, because not all strongly correlated systems are superconducting. It is here that we believe that understanding of certain *chemical* features of the unconventional superconductors gain relevance. In other words, we believe that the physics of unconventional superconductors is very strongly determined by their chemistry. This is the topic of this Review. In the following we attempt to show that many correlated-electron superconductors share two common features, (i) carrier density $\rho$ of exactly $\frac{1}{2}$ per atom, molecule or unit cell; and (ii) lattice frustration. Materials possessing these two features exhibit a strong tendency to form local spin-singlets that are the Bosonic pseudomolecules in Schafroth's theory of SC[9]. In this Review we first discuss these features in the context of the organic charge-transfer solids, and then show that similarities can be

found in several other seemingly unrelated classes of unconventional superconductors. We recognize that there exist other correlated-electron superconductors that are not $\rho = \frac{1}{2}$. Even here we believe that formation of local spin-singlets can occur and Schafroth's theory is relevant. For example, in the context of cuprates many scientists hold the opinion that preformed Cooper pairs form at temperatures much higher than $T_c$ and condense only at $T_c$. The actual demonstration of local singlets in these other superconductors will require further work.

## Charge-transfer Solids as prototype $\rho = \frac{1}{2}$ superconductors

SC in organic charge-transfer solids (CTS) has been known[10] since 1980. The two most well known families of superconducting CTS are the $(TMTSF)_2X$ and $(BEDT\text{-}TTF)_2X$, where the molecules TMTSF and BEDT-TTF constitute the active components containing the charge-carrying holes and X are closed shell anions[5]. While conducting CTS compounds exist with range of charge transfers $0.5 \leq \rho < 1$ between cations and anions, in all cases the stoichiometry is 2:1 for the cationic superconductors and 1:2 for anionic superconductors. Thus the carrier concentration per *molecule*, which is how we define $\rho$ is invariably $\frac{1}{2}$. We believe that requirement of a specific density for SC here is an important feature.

### Effective $\rho = 1$ model

The highest $T_c$ in the CTS is found in the $\kappa$-$(BEDT\text{-}TTF)_2X$, in which there occur dimers of BEDT-TTF molecules, with strong intradimer electron hoppings and weaker interdimer hoppings[11]. The dimers form anisotropic triangular lattices. At ambient pressures and low temperatures, $\kappa$-$(BEDT\text{-}TTF)_2X$ are antiferromagnetic (AFM) insulators, and under moderate pressure they become superconducting[11]. The AFM is described easily within an *effective* $\frac{1}{2}$-filled band ($\rho = 1$) Hubbard model (with each dimer an effective site) that is close to being a square lattice, given by the following Hamiltonian:

$$H = -t \sum_{\langle ij \rangle} B_{i,j} - t' \sum_{[ij]} B_{i,j} + U \sum_i n_{i\uparrow} n_{i\downarrow} \qquad (1)$$

In Eq. 1 $B_{i,j} = \sum_\sigma (c^\dagger_{j,\sigma} c_{i,\sigma} + H.c.)$ is the kinetic energy operator for the bond between sites $i$ and $j$, where $c^\dagger_{i,\sigma}$ creates an electron of spin $\sigma$ on site $i$. The sites $i$ and $j$ in $\langle ij \rangle$ are nearest neighbors on a square lattice while $[ij]$ are sites connected in the $x+y$ direction (see Fig. 3(c) in reference 11). $n_{i\sigma} = c^\dagger_{i,\sigma} c_{i,\sigma}$ is the density operator and $n_i = n_{i\uparrow} + n_{i\downarrow}$. $U$ is the on-site Coulomb interaction.

The ground state of Eq. 1 in the $t' = 0$ limit is the Neél AFM state. This had prompted some scientists to propose that pressure reduces the lattice anisotropy (increasing the isotropic character) and increases the bandwidth, and at a critical bandwidth SC dominates over AFM. The phase diagram of Eq. 1 as determined[12,13] using the using the Path Integral Renormalization Group (PIRG) method[14] is shown in Fig. 1(a). As the frustration $t'$ increases from zero, a paramagnetic metallic (PM) enters. The metal-insulator transition here may be seen in a simultaneous drop in the double occupancy ($D = \langle n_{i,\uparrow} n_{i,\downarrow} \rangle$) and the bond order ($B = \sum_\sigma \langle c^\dagger_{i,\sigma} c_{j,\sigma} \rangle$) as $U$ increases at fixed $t'$ (see Fig. 1(b) and (c)). At still larger $t'$, a non-magnetic insulator (NMI) phase which unlike the AFM phase has no long-range magnetic order[12,15,16], enters between the PM and AFM phases.

Many mean-field calculations suggested that SC occurs near the metal-insulator transition in the model (see Reference 13 for a discussion of these papers). As we have investigated Eq. 1 with a fixed number of particles, we looked for off-diagonal long range order (ODLRO)[17] by numerically calculating the pair-pair correlation function. The operator $\Delta^\dagger_{i,j}$ creates a singlet pair on lattice sites $i$ and $j$:

$$\Delta^\dagger_{i,j} = \frac{1}{\sqrt{2}} (c^\dagger_{i,\uparrow} c^\dagger_{j,\downarrow} - c^\dagger_{i,\downarrow} c^\dagger_{j,\uparrow}). \tag{2}$$

The pair-pair correlation function is then defined as

$$P(\mathbf{r}) = \frac{1}{4} \sum_\nu g(\nu) \langle \Delta^\dagger_i \Delta_{i+\mathbf{r}(\nu)} \rangle. \tag{3}$$

In Eq. 3 the sum is over the four nearest neighbor sites of the square lattice; the phase factor $g(\nu)$ determines the symmetry of the superconducting order parameter. We have performed explicit calculations of P($\mathbf{r}$) for $s$ ($g(\nu) = 1$ for all $\nu$) and $d_{x^2-y^2}$ ($g(\nu)$ alternating $\pm$ 1) pair symmetries within Eq. 1. If SC is present, $P(\mathbf{r})$ measured in the ground state must converge to a nonzero value for $|\mathbf{r}| \to \infty$. One also expects an enhancement of $P(r)$ by the

$U$ interaction. In calculations of $P(\mathbf{r})$ using exact diagonalization[18] and on larger lattices using PIRG[13], $P(\mathbf{r})$ for all $\mathbf{r}$ beyond nearest neighbor pair separation decreases continuously with increasing $U$ (see Fig. 1(d)), consistent with the absence of SC in the model. This is shown in Fig. 1(d), where we plot the pair-pair correlation $P_d(r^\star)$ for $d_{x^2-y^2}$ symmetry, where $r^\star$ corresponds to one of the longest pair separations possible on each finite lattice[13]. In Fig. 1(e) we plot the *difference* $\Delta P_d(r,U) = P_d(r,U) - P_d(r,U=0)$ showing the enhancement of the pairing over the uncorrelated model; we find no enhancement beyond nearest-neighbor distances. The small enhancement for nearest-neighbor pairs (which overlap in real space) is likely the reason that mean-field methods find SC in the model[13].

Other numerical studies going beyond the mean-field level also fail to find SC[19]. More recently, we have shown that the addition of an additional AFM Heisenberg interaction $J_{ij}$ to Eq. 1 also fails to produce SC[20]. Experimentally, the insulating phase proximate to SC in the CTS can be different from AFM, including charge-ordered CO or the so-called valence-bond-solid phase. Neither of these insulating states are accounted for within the effective $\rho = 1$ model[20].

### $\rho = \frac{1}{2}$ model and quasi-1D CTS

An alternate approach to the effective $\rho = 1$ model is the $\rho = \frac{1}{2}$ model where we consider individual molecules and not dimers as the proper units. We have done calculations within the extended Hubbard model both in one and two dimensions (1D and 2D) that show the strong tendency to form nearest neighbor spin-singlets in this case. When a nearest neighbor singlet forms between two molecules in a system with an average charge $\rho = \frac{1}{2}$, necessarily the charge density on the molecules involved in the bond is slightly increased, $\rho_+ = 0.5 + \delta$, while the charge density on the non-bonded molecules is slightly decreased, $\rho_- = 0.5 - \delta$. Thus the formation of singlet pairs in a $\rho = \frac{1}{2}$ system implies the presence of charge-ordering or at least charge-disproportionated molecules.

The general form of the Hamiltonian we consider for these systems is the following Peierls

Extended Hubbard model:

$$\begin{aligned} H &= -\sum_{\langle ij\rangle} t_{ij}(1+\alpha\delta_{i,j})B_{i,j} + \frac{1}{2}K_\alpha \sum_{\langle ij\rangle}\delta_{i,j}^2 + \beta\sum_i n_i v_i \\ &+ \frac{1}{2}K_\beta\sum_i v_i^2 + U\sum_i n_{i\uparrow}n_{i\downarrow} + V\sum_{\langle ij\rangle} n_i n_j. \end{aligned} \tag{4}$$

The terminology in Eq. 4 follows that of Eq. 1. In addition to the onsite Coulomb interaction $U$, we include in general the nearest-neighbor Coulomb interaction $V$. Electron-phonon (e-p) coupling is included in the semi-classical approximation, where $\alpha$ ($\beta$) is the inter-site (intra-site) e-p coupling constant and $K_\alpha$ ($K_\beta$) the associated spring constant. We solve Eq. 4 numerically, measuring the charge density $\langle n_i\rangle$ and bond order $\langle B_{i,j}\rangle$. The classical inter– and intra–molecular distortions $\delta_{i,j}$ and $v_i$ are determined self-consistently[21] from the equations

$$\delta_{i,j} = -\frac{\alpha}{K_\alpha}\langle B_{i,j}\rangle, \qquad v_i = -\frac{\beta}{K_\beta}\langle n_i\rangle. \tag{5}$$

Other correlation functions such as spin-spin correlations, $\langle S_i^z S_j^z\rangle = \langle (n_{i,\uparrow}-n_{i,\downarrow})(n_{j,\uparrow}-n_{j,\downarrow})\rangle$, may be measured following convergence of the iterative self-consistency procedure.

The ground state of Eq. 4 is well understood in the 1D limit where a number of different broken-symmetry phases are found. In Fig. 2 we show the phase diagram of Eq. 4 for a 1D 16 site lattice, with e-e parameters chosen as appropriate for the $(TMTTF)_2X$ group of materials[21]. The phase diagrams are plotted as a function of the normalized e-p couplings constants $\lambda_\alpha = \alpha^2/(K_\alpha t)$ and $\lambda_\beta = \beta^2/(K_\beta t)$. At $\rho = \frac{1}{2}$ there is a competition between two different insulating phases: First, the nearest-neighbor Coulomb interaction $V$ in Eq. 4 leads to a charge-ordered state (labeled "$4k_F$ CDW" in Fig. 2) with alternating charge densities large–small–large–small in the pattern "1010". In the 1D system this state occurs for $V > V_c$, where $V_c = 2t$ for $U \to \infty$, and $V_c > 2t$ for finite $U$. Sufficiently strong e-p coupling can lead to a spin-Peierls (SP) state ($4k_F$ CDW-SP in Fig. 2), where the spin-singlet bonds between the charge-rich sites alternate in strength (i.e., bond-distortion pattern "strong-strong-weak-weak", [1 = 0 = 1 – 0 – ], where a "double" bond is stronger than a "single" bond). Secondly, for $V < V_c$, a charge-ordered state with charge pattern 1100 is found. In this Bond-Charge Density Wave ("BCDW" in Fig. 2) state, nearest-neighbor singlets form between the charge-rich sites and bond orders are also necessarily modulated. In the BCDW the bond pattern

may be either "strong-undistorted-weak-undistorted", [1 = 1 – 0 $\cdots$ 0 –], or "strong-weak-strong-weak′ ", [1 = 0 $\cdots$ 0 = 1 – ], depending on the strength of e-e correlations[22]. The singlet formation in the BCDW leads to a nonmagnetic ground state with a spin gap. The SP state that is observed experimentally in the quasi-1D $\rho = \frac{1}{2}$ CTS in all cases is the BCDW and not the $4k_F$ CDW-SP. Compared to the $4k_F$ CDW, the charge density modulation in the BCDW is much smaller, and the clearest experimental signatures are the presence of a spin gap and the predicted bond distortion pattern. In materials where the bond pattern in the SP state has been measured, for example MEM$(TCNQ)_2$, the measured bond pattern is the same as that predicted for the BCDW from calculations[21].

## AFM to PEC transition and 2D CTS

In a 2D square lattice of dimers the ground state of Eq. 4 for finite $U$ and $V < V_c$ at $\rho = \frac{1}{2}$ has AFM order (see Fig. 3(a) and (b)). If sufficient lattice frustration is introduced the AFM order is expected to vanish. The lattice structure we consider here is a square lattice with dimerization along the $x$ direction. A $t'$ bond in the $x+y$ direction introduces frustration. To understand the effect of frustration we calculated charge densities, bond orders, and most importantly spin-spin correlation function as a function of $t'$. Details of these results are shown in original work[23]. Above a critical value of $t'$ a sudden change occurs in all of these correlation functions. At this transition, the AFM order shown in Fig. 3(a) and (b) gives way to the charge-ordered state shown in Fig. 3(c) and (d). Examination of the spin-spin correlations demonstrates the loss of AFM order and formation of local singlets[23].

We have termed this state a Paired Electron Crystal (PEC)[23]. In the PEC the same local charge order (CO) pattern $\cdots 1100 \cdots$ is found as in 1D. Schematic figures showing these results are shown in Fig. 3, where Fig. 3(c) shows the PEC state found under open boundary conditions and Fig. 3(d) the PEC state found under periodic boundary conditions.

The PEC state has been seen experimentally in a number of 2D CTS. One example of a class of CTS that well illustrates the AFM/PEC phenomenology as lattice frustration is varied is the Z$[Pd(dmit)_2]_2$ series[24]. Like the $\kappa$-(BEDT-TTF)$_2$X, in the Z$[Pd(dmit)_2]_2$ crystal structure $Pd(dmit)_2$ occur in dimers. Through different choices in the cation Z, which change the crystal anisotropy, a series of ground states from AFM to charge and "valence bond"

order are seen[24]. The transition between the Mott insulator with uniform dimer charges and the PEC state has also been studied experimentally[25] in $\beta$-(*meso*-DMBEDT-TTF)$_2$PF$_6$. Certain CTS with the $\kappa$-(BEDT-TTF)$_2$X structure do show CO states. For example, in $\kappa$-(ET)$_4$[M(CN)$_6$][N(C$_2$H$_5$)$_4$]·2H$_2$O (M= Co, Fe), a transition from a Mott insulating phase to a CO spin gap phase is found as the temperature goes below T=150K[26]. Here and in many other examples, evidence of fluctuating CO is found before the transition (T>150 K)[26]. Further experimental evidence for the PEC in 2D CTS is discussed in references 23 and 27.

## Model for SC

In many cases the experimentally seen PEC state is adjacent to SC. For example, under ambient pressure, EtMe$_3$P[Pd(dmit)$_2$]$_2$ has an insulating PEC ground state with inter-dimer singlet pairs (termed a valence-bond solid in Reference 24). Under a pressure of 0.18 GPa this insulating state becomes a superconducting[24]. This suggests that under a small structural modification to the material, the nearest-neighbor pairs in the PEC state can become mobile, in a realization of the Schafroth theory of local-pair SC[9,28]. In this scenario, the application of external pressure will strongly affect the the weakest bonds in the crystal lattice. The weak bonds are also those responsible for the frustration; hence one effect of pressure is to *increase* the lattice frustration. We have proposed that increased frustration allows fluctuations of the PEC ordered singlets, causing the singlet pairs to have mobility.

A simple effective model can be constructed as shown in Fig. 4. Fig. 4(a) shows schematically the PEC CO pattern in a 2D CTS crystal such as EtMe$_3$P[Pd(dmit)$_2$]$_2$. Neighboring molecules with higher charge density are singlet paired. This can be mapped to the simpler effective model shown in Fig. 4(b), where pairs of nearest neighbor occupied (unoccupied) sites are replaced by single sites with double occupancy (vacancy). Now the CO alternates (in the extreme limit) between charge densities of "2" and "0" carriers on each site. This effective model therefore has an average density of $\rho = 1$ rather than $\rho = \frac{1}{2}$, and an effective *attraction* between carriers on each site (negative $U$). The long range interactions remain

repulsive however. The Hamiltonian for this model is

$$H = -t \sum_{\langle ij \rangle} B_{i,j} - t' \sum_{[ij]} B_{i,j} - U \sum_{i} n_{i,\uparrow} n_{i,\downarrow} + V \sum_{\langle i,j \rangle} n_i n_j. \tag{6}$$

In Eq. 6, operators have the same meaning as in Eq. 1 and Eq. 4; the important distinction is that here $\rho = 1$. Similar modeling of spin-paired singlets by effective double occupancies has been done in the past by others[29,30]. The difference in our work here is that the spin-paired state is not *assumed* as in previous work, but is proved rigorously.

The lattice structure we chose is again a square lattice with bonds $t$ with a frustrating bond $t'$ in the $x + y$ direction. The $-U$ interaction here leads to a superconducting phase as expected. We calculated the SC pair-pair correlation function for on-site pairs

$$P(\mathbf{r}) = \frac{1}{N} \sum_{j} \langle c^{\dagger}_{j,\uparrow} c^{\dagger}_{j,\downarrow} c_{j+\mathbf{r},\downarrow} c_{j+\mathbf{r},\uparrow} \rangle, \tag{7}$$

and the charge structure factor

$$S(\mathbf{q}) = \frac{1}{N} \sum_{i,j} e^{i\mathbf{q}\cdot(\mathbf{r}_i - \mathbf{r}_j)} \langle (n_i - 1)(n_j - 1) \rangle, \tag{8}$$

as a function of $t'$ ($N$ is the number of lattice sites). For small $t'$ $S(\mathbf{q})$ peaks at $\mathbf{q} = (\pi, \pi)$ consistent with the checkerboard CO shown in Fig. 4(b). At a critical $t'$ a sudden decrease of $S(\pi, \pi)$ coincident with an increase of $P(\mathbf{r})$ indicates a transition from CO to SC. We show in Fig. 4(c) and (d) the ground state phase diagram of Eq. 6 from exact calculations on a 16 site lattice[28]. While this simple model does not capture details of the SC state (the pairing is an on-site singlet), the calculated frustration induced transition between CO and SC reproduces qualitatively the experimentally observed transition from a spatial broken symmetry state to SC in many CTS superconductors.

The mechanism for the proposed transition to the superconducting state has similarities with some other proposed mechanisms. We have already mentioned the relationship between our work and Schafroth's idea of the condensation of charged Bosons. Our work may also be considered as an extension of the Resonating Valence Bond theory of SC[31] to the specific case of $\rho = \frac{1}{2}$. Finally, we mention the work by Dunne and Brändas[32,33], who have proposed that condensation to the superconducting state can occur if the short-range component of the Coulomb repulsion is screened and the long range component is attractive. In our case this

nonlocal effective attraction arises from the antiferromagnetic spin-spin correlations between neighboring sites in the $\rho = \frac{1}{2}$ lattice. One difference between our work and that by Dunne and Brändas is that in addition to the latter being derived from the large eigenvalue of the density matrix and thus exhibiting ODLRO, in our case lattice frustration plays a key role in driving the superconducting transition, while it is alternancy symmetry rather than frustration that is important in the model of Dunne and Brändas. Further work is necessary to reveal the similarities and differences between these models.

## The ubiquity of unconventional $\rho = \frac{1}{2}$ superconductors

In this section we point out the preponderance of correlated-electron $\rho = \frac{1}{2}$ superconductors. In many cases, phenomenology similar to that described above for the CTS is observed, for example charge ordering with charge periodicity $\cdots 1100 \cdots$. This is despite radically different material characteristics (organic versus inorganic and dimensionality). Although the materials listed below have attracted strong interest individually, until now the carrier density itself was not considered an important variable.

### Spinels

Spinels are inorganic ternary compounds $AB_2X_4$, with the B-cations as the active sites. $LiTi_2O_4$ [3], $CuRh_2S_4$ and $CuRh_2Se_4$ [4] are the only three spinels that have been confirmed to be superconductors. $Ti^{3.5+}$ in $LiTi_2O_4$ has one d-electron per two Ti-ions; $Rh^{3.5+}$ in $CuRh_2S_4$ and $CuRh_2Se_4$ is in its low-spin state and has one d-hole per two Rh-ions. Further, Jahn-Teller distortion removes $t_{2g}$ degeneracy, creating a true $\rho = \frac{1}{2}$ d-band of one specific symmetry. The crucial role of carrier density is demonstrated from the large $T_c = 11$ K in $LiTi_2O_4$ on the one hand, and only short-range magnetic correlations down to 20 mK in $LiV_2O_4$. $T_c/T_F$ is recognized to be large in $LiTi_2O_4$, and the mechanism of SC here remains controversial. Importantly, static lattice distortions give a three dimensional (3D) PEC with nearest-neighbor pairing in $CuIr_2S_4$ [34] and $LiRh_2O_4$ [35], which are isoelectronic with the superconductors. This 3D PEC has the same *CO periodicity as in the CTS.* Pressure-dependent measurements and search for SC in the last two compounds are called for.

### $Na_xCoO_2{\cdot}yH_2O$

Layered cobaltates are unique in that $\rho$ can be varied over a wide range by varying $x$[36]. We have shown that the $\rho$-dependent electronic behavior of anhydrous $Na_xCoO_2$ can be explained through an identical mechanism as in the CTS[37]. In the hydrated superconducting Na-cobaltate with $x = 0.35$, the water enters as $H_3O^+$ ions, and the Co valence is set by both Na doping and the amount of $H_3O^+$ . Experimental measurements of the actual valence state of the Co atoms in the superconducting compound find $Co^{3.5+}$, corresponding to $\rho = \frac{1}{2}$[38].

### $Li_{0.9}Mo_6O_{17}$

This material has attracted attention because of its unusually large upper critical field[39]. Very little is currently known about the superconducting state of this material. The Mo-valence of nearly 5.5 however requires equal admixing of $4d^1$ ($Mo^{5.0+}$) and $4d^0$ ($Mo^{6.0+}$). It is conceivable that the large upper critical field is due to the local singlets with molecular dimension.

### Metal-intercalated phenacenes

SC has very recently been found in metal-intercalated phenanthrene[40], picene[7], coronene[7] and dibenzopentacene[41]. In every case "doping" with 3 electrons per molecule is essential for SC. The lowest unoccupied molecular orbital (LUMO) and the next higher MO (LUMO+1) are unusually close in these molecules (in coronene they are degenerate). It has been shown that with 3 electrons added the electron populations of the LUMO and LUMO+1 are almost 1.5 each due to combined bandwidth and correlation effects, and that this strongly suggests that the mechanism of SC in these doped polycyclic aromatics and the CTS are same[42].

## CONCLUSIONS

Correlated-electron SC continues to be a formidable problem in spite of decades-long intensive research. SC at a particular carrier density, as well as perceptible similarity between different families of correlated superconductors can hardly be coincidences. We believe

that both features indicate that the physics of these materials (antiferromagnetism, charge-ordering, SC) is strongly linked to their chemistry (stoichiometry and carrier density). Our proposed mechanism of SC, though far from complete, offers a single unified approach to a wide variety of systems, and can perhaps even be extended to the more popular cuprates and Fe-compounds, where too local singlet-formation has been suggested by many authors. The strong role of electron-phonon interactions, as observed in many experiments, is to be anticipated at $\rho = \frac{1}{2}$ (see Figs. 2 and 3), in spite of the large $T_c/T_F$. Our work provides strong motivation for focused research for a theory of correlated-electron SC in $\rho = \frac{1}{2}$.

## ACKNOWLEDGMENTS

The present review paper grew out of an invited talk presented by one of us (SM) at the 8th Congress of the International Society of Theoretical Chemical Physics, held in Budapest, Hungary, August 25-31, 2013. SM is grateful to Professor Miklos Ketesz of Georgetown University) for organizing the session on Solid State Chemistry and for inviting him. The work by the authors was supported by the Department of Energy grant DE-FG02-06ER46315. SM acknowledges partial support from NSF Grant No. CHE-1151475.

# References


1. Bednorz, J. G., Müller, K. A., Z. Phys. B, **1986**, 64, 189–193.
2. Wen, H.-H., Li, S., Annu. Rev. Condens. Matter Phys., **2011**, 2, 121–140.
3. Johnston, D. C., Prakash, H., Zachariahsen, W. H., Viswanathan, R., Mater. Res. Bull., **1973**, 8, 77.
4. Hagino, T., et al., Phys. Rev. B, **1995**, 51, 12673–12684.
5. Ishiguro, T., Yamaji, K., Saito, G., Organic Superconductors, New York: Springer-Verlag, **1998**.
6. Capone, M., Fabrizio, M., Castellani, C., Tosatti, E., Rev. Mod. Phys., **2009**, 81, 943.
7. Kubozono, Y., et al., Phys. Chem. Chem. Phys., **2011**, 13, 16476–16493.
8. Uemura, Y. J., Le, L. P., Luke, G. M., Sternlieb, B. J., Wu, W. D., Brewer, J. H., Riseman, T. M., Seaman, C. L., Maple, M. B., Ishikawa, M., Hinks, D. G., Jorgensen, J. D., Saito, G., Yamochi, H., Phys. Rev. Lett., **1991**, 66, 2665–2668.
9. Schafroth, M. R., Phys. Rev., **1955**, 100, 463.
10. Ribault, M., Pouget, J. P., Jerome, D., Bechgaard, K., J. Phys. (Paris) Lett., **1980**, 41, L607–610.
11. Kanoda, K., Kato, R., Annu. Rev. Condens. Matter Phys., **2011**, 2, 167.
12. Morita, H., Watanabe, S., Imada, M., J. Phys. Soc. Jpn., **2002**, 71, 2109–2112.
13. Dayal, S., Clay, R. T., Mazumdar, S., Phys. Rev. B, **2012**, 85, 165141.
14. Kashima, T., Imada, M., J. Phys. Soc. Jpn., **2001**, 70, 2287–2299.
15. Kashima, T., Imada, M., J. Phys. Soc. Jpn., **2001**, 70, 3052.
16. Mizusaki, T., Imada, M., Phys. Rev. B, **2006**, 74, 014421.

17. Yang, C. N., Rev. Mod. Phys., **1962**, 34, 694.

18. Clay, R. T., Li, H., Mazumdar, S., Phys. Rev. Lett., **2008**, 101, 166403.

19. Tocchio, L. F., Parola, A., Gros, C., Becca, F., Phys. Rev. B, **2009**, 80, 064419.

20. Gomes, N., Clay, R. T., Mazumdar, S., J. Phys.: Condens. Matter, **2013**, 25, 385603.

21. Clay, R. T., Mazumdar, S., Campbell, D. K., Phys. Rev. B, **2003**, 67, 115121.

22. Ung, K. C., Mazumdar, S., Toussaint, D., Phys. Rev. Lett., **1994**, 73, 2603–2606.

23. Li, H., Clay, R. T., Mazumdar, S., J. Phys.: Condens. Matter, **2010**, 22, 272201.

24. Tamura, M., Kato, R., Sci. Technol. Adv. Mater., **2009**, 10, 024304.

25. Okazaki, R., et al., Phys. Rev. Lett., **2013**, 111, 217801.

26. Ota, A., et al., Chem. Mater., **2007**, 19, 2455.

27. Dayal, S., Clay, R. T., Li, H., Mazumdar, S., Phys. Rev. B, **2011**, 83, 245106.

28. Mazumdar, S., Clay, R. T., Phys. Rev. B, **2008**, 77, 180515(R).

29. Alexandrov, A., Ranninger, J., Phys. Rev. B, **1981**, 23, 1796–1801.

30. Micnas, R., Ranninger, J., Robaszkiewicz, S., Rev. Mod. Phys., **1990**, 62, 113.

31. Anderson, P. W., Science, **1987**, 235, 1196.

32. Dunne, L. J., Brändas, E. J., Int. J. Quant. Chem., **2013**, 113, 2053.

33. Dunne, L. J., Brändas, E. J., Adv. Quant. Chem., **2013**, 66, 1.

34. Radaelli, P. G., et al., Nature, **2002**, 416, 155–158.

35. Okamoto, Y., et al., Phys. Rev. Lett., **2008**, 101, 086404.

36. Foo, M. L., et al., Phys. Rev. Lett., **2004**, 92, 247001.

37. Li, H., Clay, R. T., Mazumdar, S., Phys. Rev. Lett., **2011**, 106, 216401.

38. Barnes, P. W., et al., Phys. Rev. B, **2005**, 72, 134515.

39. Mercure, J.-F., et al., Phys. Rev. Lett., **2012**, 108, 187003.

40. Wang, X., et al., Nature Communications, **2011**, 2, 507.

41. Xue, M., et al., Scientific Reports, **2012**, 2, 389.

42. Dutta, T., Mazumdar, S., preprint http://arxiv.org/abs/1311.3931.

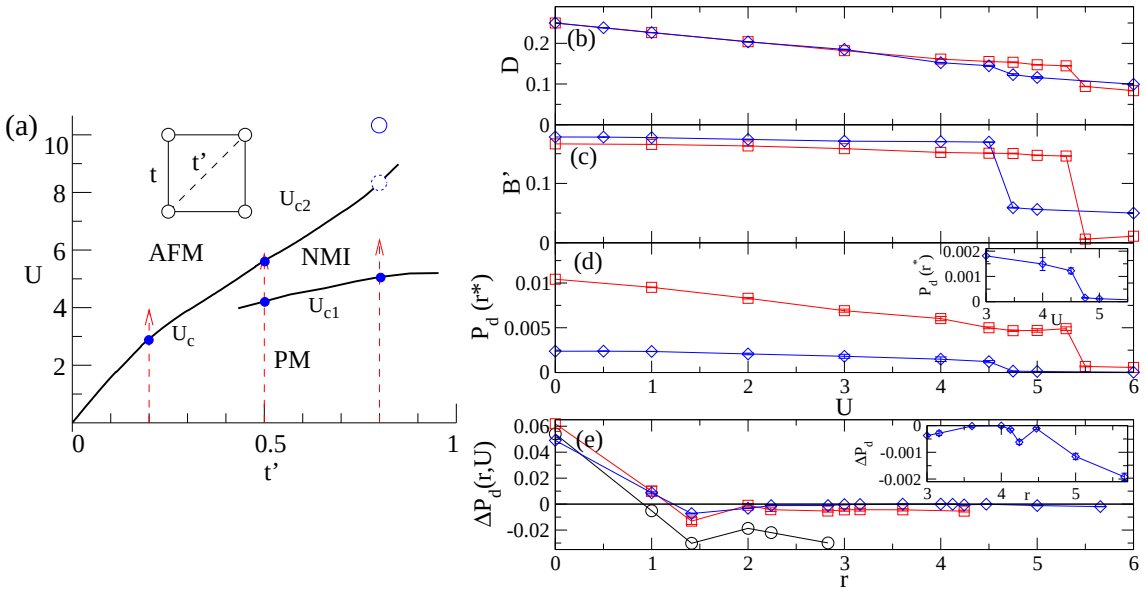


Figure 1: (a) Phase diagram of the 2D $\rho = 1$ effective model of Eq. 1 based on PIRG calculations[13]. Filled points are determined using PIRG and finite-size scaling. The NMI/AFM phase boundary at $t'$=0.8 is more uncertain; the solid circle there is the upper bound from 4×4 exact diagonalization, and the dotted circle is the expected boundary in the thermodynamic limit. (b)-(d) Double occupancy, $t'$ bond order, and long-distance $d_{x^2-y^2}$ pair-pair correlation function, respectively, as a function of $U$ for $t'$=0.5. Squares (diamonds) are for 6×6 (8×8) lattices. (e) Enhancement of the pair-pair correlation over the uncorrelated system. Here circles are exact results for the 4×4 lattice. Reproduced from Reference 13.

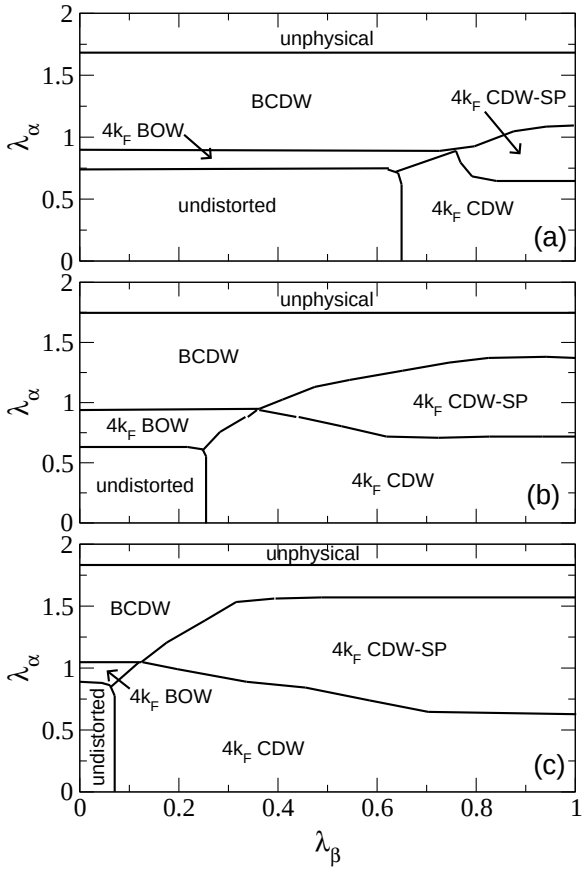


Figure 2: Phase diagram of the 1D model of Eq. 4 based on 16-site exact calculations for $U = 8$ and (a) $V = 2$, (b) $V = 3$, and (c) $V = 4$. $\lambda_\alpha$ and $\lambda_\beta$ are the normalized inter- and intra-site e-p couplings (see text). Reproduced from Reference 21.

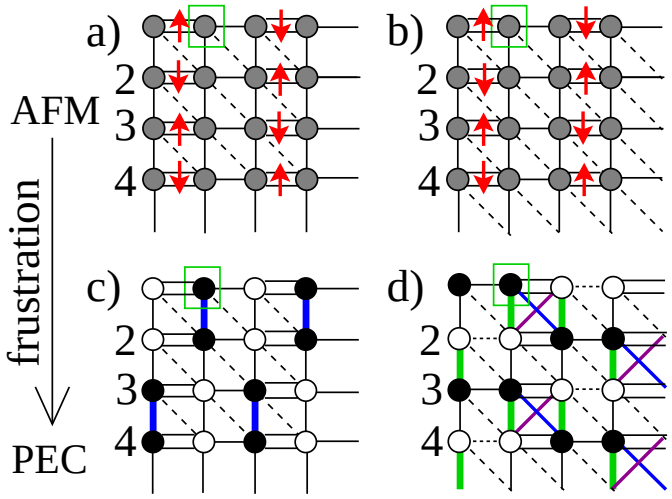


Figure 3: The AFM to PEC transition as seen in exact 4×4 cluster calculations for dimerized $\rho = 0.5$ systems. Panels (a) and (c) correspond to calculations in open boundary conditions, while those in (b) and (d) are from periodic boundary calculations. Grey circles correspond to sites with charge density $\rho = 0.5$; black (white) circles to sites with $\rho > 0.5$ ($\rho < 0.5$). The arrows in (a) and (b) indicate the observed AFM pattern observed in spin correlations. The heavy lines in (c) and (d) indicate the location of nearest-neighbor singlet bonds formed in the PEC state. Reproduced from Reference 23.

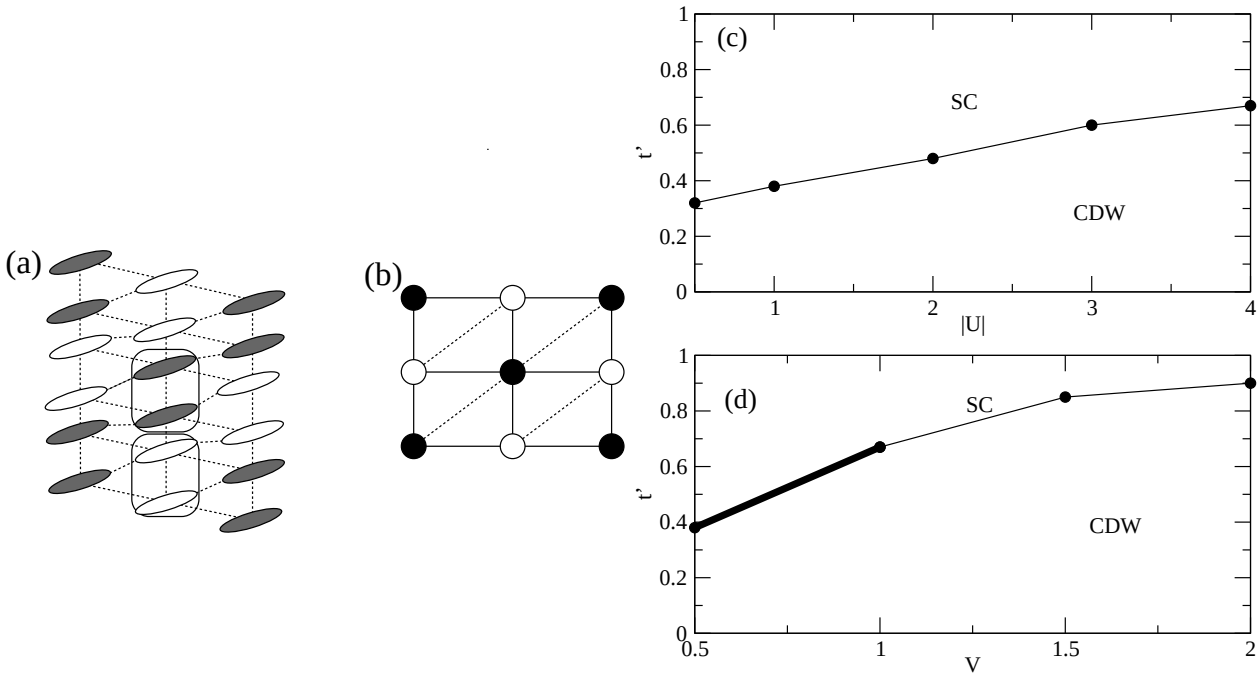


Figure 4: (a) Schematic picture of the PEC insulating state in a 2D CTS crystal. Molecules with $\rho > 0.5$ ($\rho < 0.5$) are drawn with filled (open) symbols. (b) Equivalent CO state in the effective $\rho = 1$ model. Filled (open) circles correspond to pairs of molecules with more (less) charge. (c) Phase diagram of the effective model (Eq. 6) as a function of $t'$ and $|U|$, and (d) $t'$ and $|V|$. Reproduced from Reference 28.